 doi: 10.1111/cpf.12410

Circumferential strain by velocity vector imaging and speckle-tracking echocardiography: validation against sonomicrometry in an aortic phantom

Johan Petrini[1,2], Maria J. Eriksson[1,3], Kenneth Caidahl[1,3] and Matilda Larsson[1,4]

[1]Department of Molecular Medicine and Surgery, Karolinska Institutet, [2]Department of Clinical Physiology, Södersjukhuset, [3]Department of Clinical Physiology, Karolinska University Hospital, and [4]Department of Medical Engineering, School of Technology and Health, KTH Royal Institute of Technology, Stockholm, Sweden

Correspondence
Johan Petrini, Department of Molecular Medicine and Surgery L1:00, Karolinska University Hospital, SE 171 76 Stockholm, Sweden
E-mail: johan.petrini@ki.se

Accepted for publication
Received 27 April 2016;
accepted 22 November 2016

Key words
aortic phantom; arterial strain; sonomicrometry; speckle-tracking

Summary

Background Evaluation of arterial deformation and mechanics using strain analysis on ultrasound greyscale images has gained increasing scientific interest. The aim of this study was to validate *in vitro* measurements of circumferential strain by velocity vector imaging (VVI) and speckle-tracking echocardiography (STE) against sonomicrometry as a reference method.

Method Two polyvinyl alcohol phantoms sized to mimic the descending aorta were constructed and connected to a pulsatile flow pump to obtain high-resistance flow profiles. The ultrasound images of the phantom used for strain analyses were acquired with a transesophageal probe. Global and regional circumferential strains were estimated using VVI and STE and were compared with the strain acquired by sonomicrometry.

Results Global circumferential peak strain estimated by VVI and STE correlated well to sonomicrometry ($r = 0{\cdot}90$, $P \leq 0{\cdot}001$; and $r = 0{\cdot}97$, $P \leq 0{\cdot}01$) with a systematic bias of $-0{\cdot}78\%$ and $+0{\cdot}63\%$, respectively. The reference strain levels were 1·07–2·54%. Circumferential strain values obtained by VVI were significantly lower than those obtained by STE (bias $-1{\cdot}41\%$, $P \leq 0{\cdot}001$).

Conclusion Global circumferential strain measured by VVI and STE correlates well with sonomicrometry. However, strain values obtained by VVI and STE differ significantly, which should be taken into consideration when comparing results from studies using different software for aortic strain measurements.

Introduction

Arterial stiffness is an important risk factor for cardiovascular events and morbidity (Mancia *et al.*, 2007; Cavalcante *et al.*, 2011). Decreased arterial elasticity causes higher pulse pressure, higher after-load and lower left ventricular myocardial perfusion pressure (Laurent *et al.*, 2006). The methods for measuring elastic properties of aorta and large arteries vary in clinical practice and research. Recently, analyses of local arterial mechanics expressed as strain in different vascular territories have generated interest (Teixeira *et al.*, 2016). This has been enabled by development of algorithms for evaluation of arterial images based on ultrasound or magnetic resonance (van Prehn *et al.*, 2009; Avril *et al.*, 2011; Yang & Ha, 2015) and availability of several commercial software packages, for example speckle-tracking echocardiography (STE) and velocity vector imaging (VVI).

VVI, which combines the tracking of speckle patterns and border detection algorithms performed with Fourier techniques, has been validated in an animal heart model (Pirat *et al.*, 2008) and compared with other speckle-tracking techniques in cardiac patients (Kim *et al.*, 2009a,b). With VVI, the tissue velocity is displayed as a vector showing the amplitude and direction of the movement. VVI has been applied *in vivo* for circumferential strain analyses of the ascending (Wang *et al.*, 2009) and descending aorta (Kim *et al.*, 2009a,b; Petrini *et al.*, 2010, 2014) as well as the common carotid artery (Cho *et al.*, 2010; Ma *et al.*, 2012).

STE uses the tracking of speckles in the ultrasound image to estimate tissue motion and deformation (Leitman *et al.*, 2004; Perk *et al.*, 2007; Pirat *et al.*, 2008) and has been used and validated mainly in cardiac applications (D'Hooge *et al.*, 2002) but also for the estimation of stiffness of the abdominal aorta (Oishi *et al.*, 2008). For the aortic application, STE has been

validated in an aneurysm model using laser scan micrometry in a three-dimensional set-up (Bihari *et al.*, 2013). Although phantom studies of different vascular segments have been performed (Ribbers *et al.*, 2007; Larsson *et al.*, 2011, 2015), no phantom validations of STE and VVI strain assessment applied to ultrasound images acquired by a transesophageal echocardiography (TEE) probe have been published.

The aim of this experimental study was to validate circumferential strain measurements obtained by VVI and STE applied to TEE ultrasound greyscale images, using sonomicrometry as a reference method.

Methods

A dynamic set-up (Larsson *et al.*, 2015) comprising a gel phantom connected to a programmable pulsatile flow pump was built to validate VVI and STE results experimentally using sonomicrometry.

Phantom fabrication

Two *in vitro* phantoms mimicking the descending aorta were constructed using a water solution of 13% (mass %) polyvinyl alcohol (PVA) (Sigma-Aldrich, St. Louis, MO, USA) and 1% (mass %) graphite powder with particle size <50 μm (Merck KGaA, Darmstadt, Germany), as described previously (Larsson *et al.*, 2015). This created a phantom aorta with an outer diameter of 20 mm, an inner diameter of 14 mm and a wall thickness of 3 mm. At each end of the phantom, fixing collars with an outer diameter of 28 mm were formed. The length of the phantom was 150 mm.

The mould containing the PVA/graphite solution was first stored in a freezer for 12 h at ≈ −20°C and then thawed at room temperature (≈ +20°C) for 12 h, which completed one freeze–thaw cycle. The number of applied freeze–thaw cycles determined the elasticity of the phantom; that is, a large number of cycles resulted in a low elasticity and vice versa. The two phantoms were constructed using three freeze–thaw cycles to obtain phantoms with mechanical properties similar to aortic tissue (Fromageau *et al.*, 2007).

At completion of freeze–thaw cycles, the phantoms were mounted in a polyvinyl chloride (PVC) box (110 mm × 140 mm × 150 mm) by squeezing the fixing collars between two plastic discs, as illustrated in Fig. 1. To avoid reflections from the PVC box, the bottom and the sides of the box were covered with a 3-mm-thick rubber layer. Water was then poured into the PVC box up to a level ≈10 mm above the phantom.

Experimental set-up

The phantoms were connected to a CompuFlow 1000MR pulsatile flow pump (Shelley Medical Imaging Technologies, Ontario, Canada). The pump was programmed to generate two different high-resistance flow profiles (Fig. 2) at

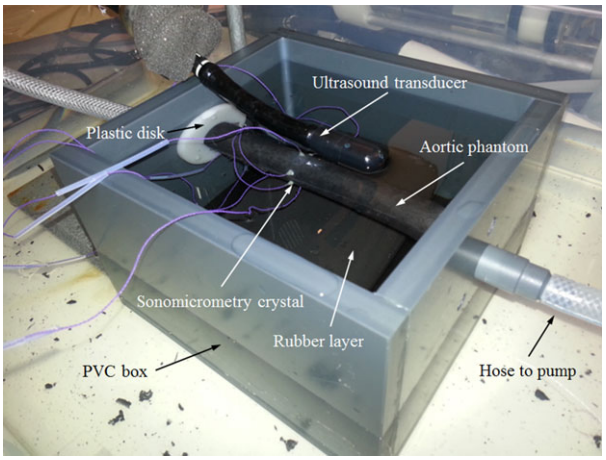

Figure 1 Close-up of the aortic phantom in the polyvinyl chloride (PVC) box with sonomicrometry crystals attached on the outer surface of the phantom and the transesophageal ultrasound probe fixed 5 mm above the phantom.

75 cycles min^{-1} with peak flows at 14, 21, 28 and 35 ml s^{-1}. A trigger signal marking the start of the pump cycle was recorded on the ECG channel of the ultrasound machine. A solution of 40% glycerine (Acros Organics, Geel, Belgium) and 60% water was used to mimic the blood. Before starting the experiments, a preprogrammed purge procedure was performed to remove air bubbles from the blood-mimicking fluid.

Data acquisition

For VVI analysis, two-dimensional ultrasound short-axis images of the phantoms were obtained using a Sequoia c512 ultrasound scanner (Siemens Medical Systems, Mountain View, CA, USA) with a TEE probe having a centre frequency of 7 MHz. The TEE probe was fixed in the water at a distance of 5 mm above the phantom using a tripod holder (Fig. 1). Images were acquired throughout one pump cycle with a mean frame rate of 89 Hz and the focus point positioned at the far wall of the phantoms. For STE analysis, the procedure was repeated using a Vivid 7 ultrasound scanner (GE Healthcare, Milwaukee, WI, USA) with a TEE probe having a centre frequency of 6 MHz (mean frame rate 109 Hz). Figure 3 shows an example of greyscale short-axis images from one of the phantoms. All ultrasound images were acquired by the same experienced investigator.

Reference strain values were assessed using a sonomicrometry system at a sampling rate of 200 Hz (Sonometrics, London, ON, Canada). Six sonomicrometry crystals were glued to the phantom surface using cyanoacrylate glue (Super glue, Loctite, Düsseldorf, Germany) to acquire data for reference circumferential strain. The crystals had a diameter of 1 mm and were glued on the outer surface of the phantom wall, 60° apart in the short-axis view (Fig. 3). To avoid sound interference, the sonomicrometry system was switched off during ultrasound image acquisition and vice versa. Ultrasound

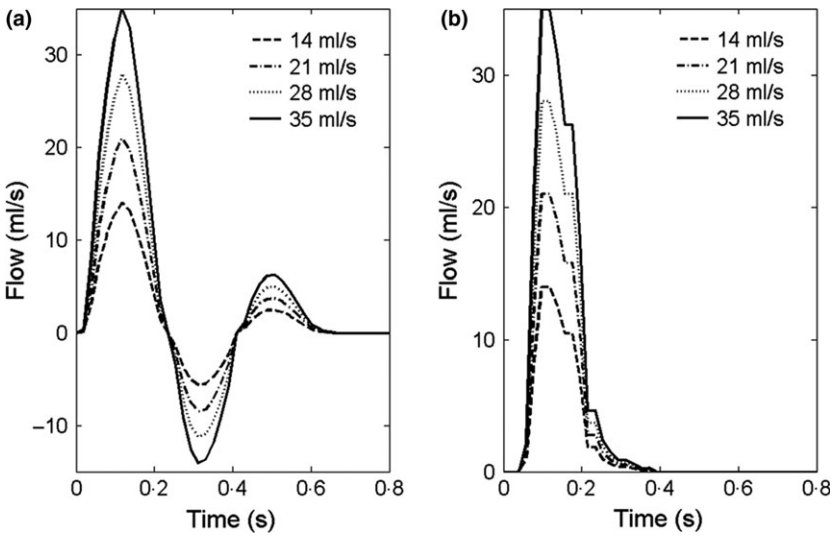

Figure 2 The two different high-resistance flow profiles (a, b) at different flow rates used in the experiments.

imaging was performed just parallel to the short-axis plane containing the sonomicrometry crystals to avoid crystal influence in the ultrasound images.

Sonomicrometry

The intercrystal displacement curves between crystals c_1 and c_2, c_2 and c_3, c_3 and c_4, c_4 and c_5, c_5 and c_6, and c_6 and c_1 were median filtered with a filter length of 35 ms to reduce noise. Subsequently, the curves were averaged over six pump cycles. Reference circumferential strain from sonomicrometry was calculated in six short-axis segments of the phantom, each corresponding to 60° along the circumference (Fig. 3a). For each segment S_i, strain (ε) was calculated as:

$$\varepsilon(t) = \frac{D_{i-j}(t) - D_{i-j}(0)}{D_{i-j}(0)}$$

where t was the time in the pump cycle, and D_{i-j} was the intercrystal displacement between the adjacent crystals c_i and c_j along the circumference with i–j = 1–2, 2–3, 3–4, 4–5, 5–6, and 6–1. Global circumferential strain by sonomicrometry was calculated as the mean for the whole circumference in the six-segment model (Fig. 4a).

Velocity vector imaging

The collected digital phantom images from the Sequoia c512 were analysed offline using Syngo US WP 3.0 VVI (Siemens Medical Systems, Mountain View, CA, USA) according to the procedure that we previously described when analysing VVI of the descending aorta *in vivo* (Petrini *et al.*, 2010) (Fig. 4b). In brief, the inner border of the phantom was traced manually. Global and regional (according to the six segments in Figs 3a and 4b) peak circumferential strain (VVI strain) was calculated automatically, and the strain values were exported as text files.

Speckle-tracking echocardiography

The collected phantom data from Vivid 7 were analysed offline using EchoPAC BT-11 (GE Healthcare, Milwaukee, WI, USA). A region of interest (ROI) with the smallest possible ROI width (Fig. 4c) was selected by manual tracing of the inner lumen border of the phantom. Because of the lumen of the phantom, the 'small animal' software as default for the analysis was used. Global and regional (according to the six segments in Fig. 4c) peak circumferential strain was then calculated automatically, and the strain values were exported as text files.

Statistics

Analyses were performed using commercially available SPSS software (version 22; IBM Corp., Armonk, NY, USA). Data are presented as mean ± SD or mean [range].

VVI and STE peak strains were correlated with reference peak strains obtained by sonomicrometry and each other using the Pearson correlation coefficient. A paired t-test was used to test whether there was a significant bias in the values obtained by VVI/STE and sonomicrometry. Linear regression analysis was used to analyse the strain–flow relationship and to derive a regression equation for estimation of strain with higher flow rate.

Results

Strain values, bias and correlation coefficients for the comparisons of peak circumferential strain measured by VVI and STE with the reference strain values obtained by sonomicrometry are presented in Tables 1 and 2. Table 2 shows biases between reference sonomicrometry strain and strain values by VVI and STE, both global and regional for each segment, as a mean for all peak flows and flow profiles in both phantoms.

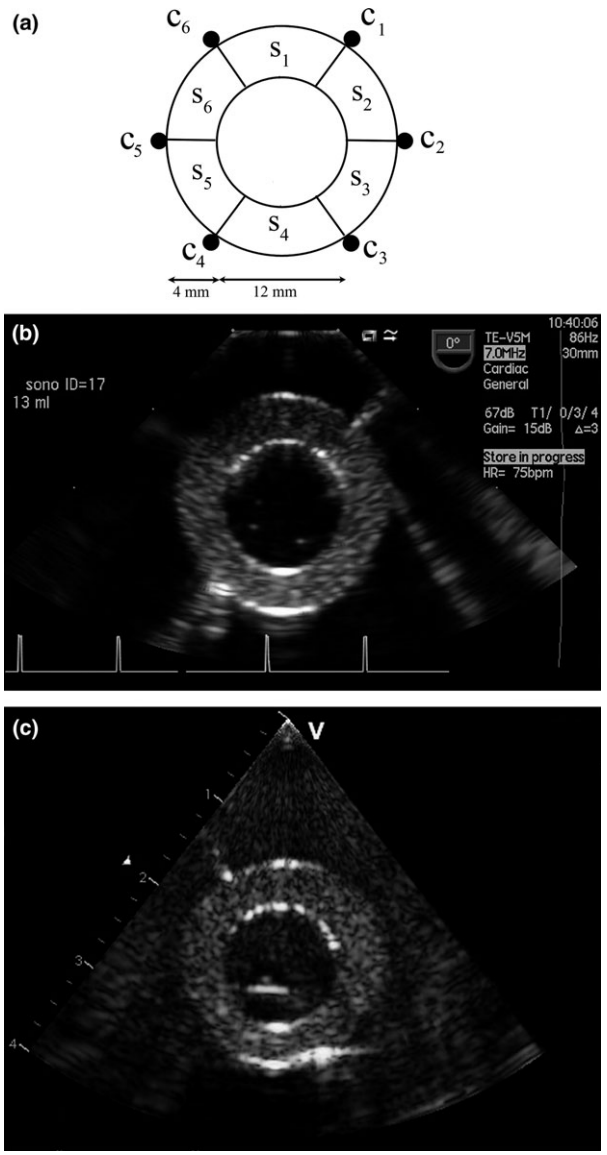

Figure 3 Schematic illustration of the cross section of the aortic phantom divided into six segments according to the placement of the sonomicrometry crystals (c_1–c_6) (a). Ultrasound short-axis images of the aortic phantom (image depth 30 mm) acquired using the Sequoia c512 (b) and Vivid 7 (c) scanners.

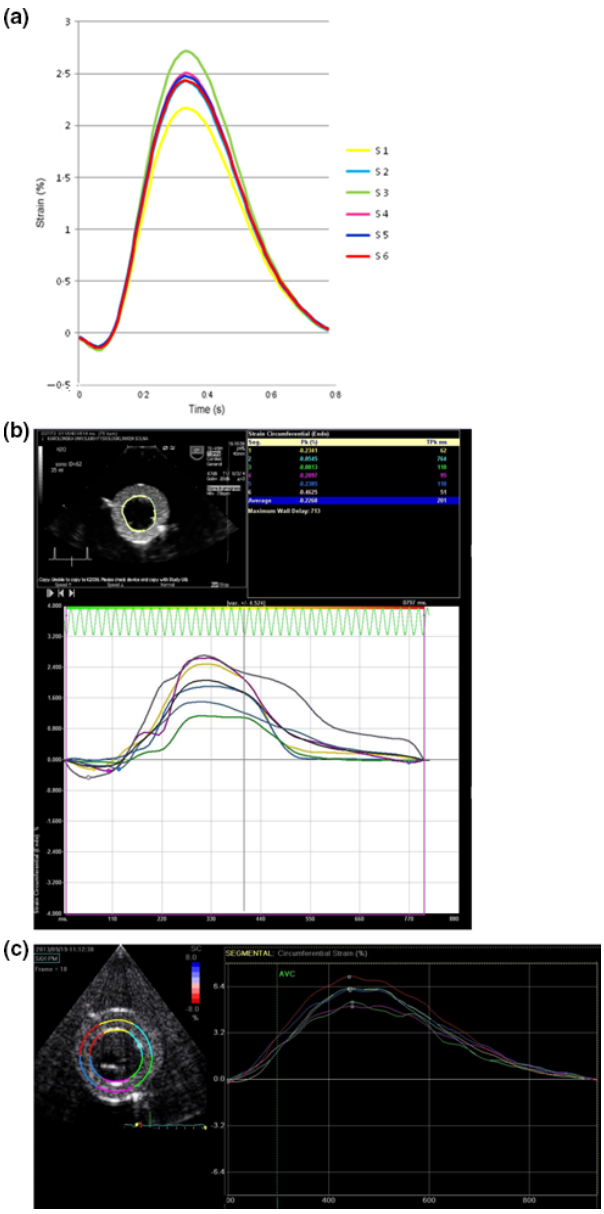

Figure 4 Curves of regional circumferential strain (coloured curves). The numbers correspond to the segments in Fig. 3a measured by sonomicrometry (a), VVI (black curve represents global circumferential strain) (b) and STE (c).

Global peak strain measured by VVI correlated strongly with reference strain (r = 0·90, P≤0·001) (Fig. 5a). However, it was significantly lower than the reference peak strain with a bias of −0·78% (SD 0·27) (P≤0·001). The differences in global VVI and reference peak strain were independent of the strain amplitude (Table 1). The global peak strain measured by STE was significantly higher (P≤0·001) than the reference peak strain with a bias of 0·63% (SD 0·30), but there was still a strong correlation between the two methods (r = 0·97, P≤0·01) (Fig. 5b). These differences increased with increasing strain amplitude (Table 1) in the measured reference strain level of 1·07–2·54%. Figure 6 shows the mean global circumferential strain curves obtained by VVI, STE and sonomicrometry for the two phantoms and two flow profiles at a flow rate of 35 ml s^{-1}. Figure 7 illustrates graphically the relationships between strain values and peak flow, and the regression formulas, with calculated strain values at higher (extrapolated) flow volumes (shown in Table 3).

The regional peak strain estimates for the six segments showed overall weaker correlations with the corresponding regional reference strain than the global strain estimates did. For two segments (S_1 and S_4), neither nonzero bias nor correlation was found to be significant between the estimation by STE and the reference strain. Eight regional strain estimates by STE and one by VVI showed negative peak strain values,

Table 1 Reference strain by sonomicrometry and strain measured by velocity vector imaging (VVI) and speckle-tracking echocardiography (STE) in the two different phantoms using the two different flow profiles at increasing flows.

Peak flow (ml s^{-1})	14	21	28	35
Phantom 1				
Sono strain (%)	1·07 [1·04–1·09]	1·63 [1·56–1·69]	2·01 [1·99–2·03]	2·45 [2·20–2·49]
VVI strain (%)	0·42 [0·38–0·46]	0·93 [0·78–1·08]	1·20 [1·19–1·21]	1·95 [1·82–2·08]
STE strain (%)	1·47 [1·35–1·58]	2·13 [2·05–2·20]	2·76 [2·73–2·79]	3·56 [3·50–3·63]
Phantom 2				
Sono strain (%)	1·07 [1·05–1·09]	1·58 [1·56–1·59]	2·02 [2·00–2·04]	2·54 [2·51–2·57]
VVI strain (%)	0·23 [0·22–0·24]	0·73 [0·45–1·00]	0·95 [0·72–1·17]	1·70 [1·31–2·09]
STE strain (%)	1·49 [1·29–1·68]	1·84 [1·58–2·11]	2·70 [2·65–2·74]	3·42 [3·40–3·44]

Mean [range flow profile a and b].

Table 2 Global and regional (S_1–S_6) strain estimation results for velocity vector imaging (VVI) and speckle-tracking echocardiography (STE) compared with the reference strain measured by sonomicrometry.

	VVI		STE	
	Bias % (SD)	*r*	Bias % (SD)	*r*
Global strain	−0·78 (0·27)*	0·90***	0·63 (0·30)**	0·97***
Strain S_1	−0·86 (0·59)***	0·70**	0·36 (0·86)	0·30
Strain S_2	−1·29 (0·44)***	0·74***	2·01 (1·27)***	0·78***
Strain S_3	−1·36 (0·50)***	0·67**	0·83 (2·06)*	0·73**
Strain S_4	−0·44 (0·63)*	0·83***	−0·94 (2·77)	−0·18
Strain S_5	−1·02 (0·43)***	0·78***	1·38 (1·61)**	0·53*
Strain S_6	−1·06 (0·62)***	0·70**	1·16 (0·95)***	0·86***

Bias (VVI/STE versus sonomicrometry) and Pearson correlation coefficients (r) for mean peak circumferential strain for two phantoms, two flow profiles and four peaks flows (n = 16). Significance levels for correlation coefficients and nonzero bias are marked with asterisks. SD: standard deviation.
*P≤0·05, **P≤0·01, ***P≤0·001.

whereas the sonomicrometry peak strain was positive for all segments. In VVI, poor quality tracking in a solitary segment was easily detected as a 'noisy' curve, often with a peak strain occurring at a different time than in the other segments. In STE, the curves were smooth, and peak strain occurred at the same time in all segments, even if STE indicated negative strain where the reference strain was positive.

Comparison of global peak circumferential strain measured by STE and VVI showed that strain by STE was significantly higher (P≤0·001) than the VVI peak strain with a bias of 1·41% (SD 0·39) and that there was a significant correlation between the two methods (r = 0·88, P≤0·001).

Discussion

We showed that global circumferential strain estimated by VVI and STE correlated strongly with strain measured by sonomicrometry in this experimental set-up that mimics the

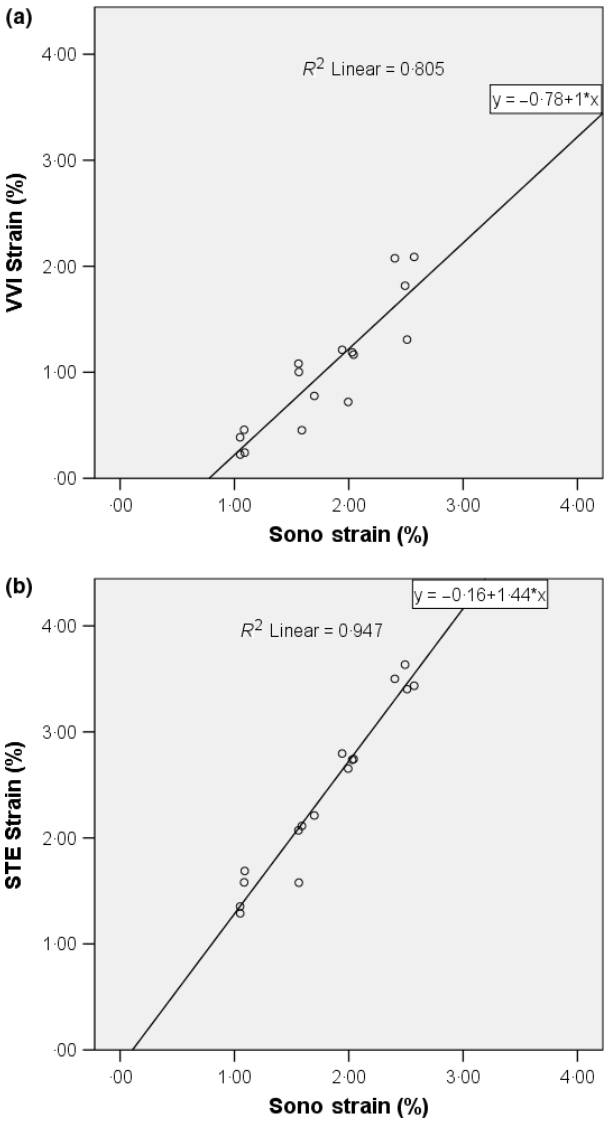

Figure 5 Correlation of global strain (%) for VVI (a) and sonomicrometry (Sono). Correlation of global strain (%) for STE (b) and sonomicrometry. Each point in the graphs represents one phantom, peak flow and flow profile (n = 16).

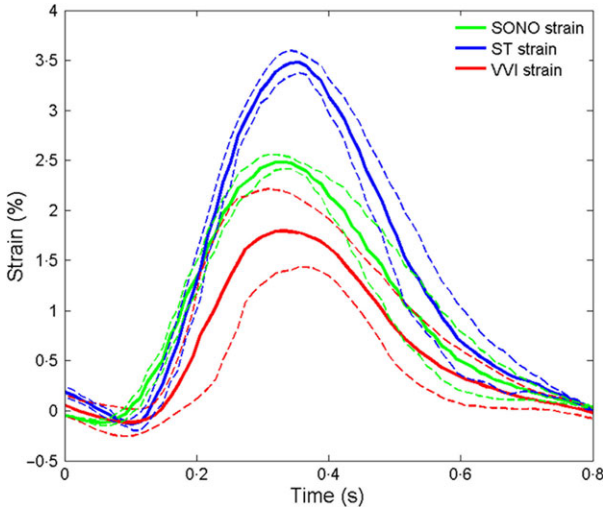

Figure 6 Mean global circumferential strain by sonomicrometry (green), STE (blue) and VVI (red) for two phantoms and two flow profiles at 35 ml s^{-1}. The dotted lines represent the mean ± one standard deviation.

measurement of elasticity in the descending aorta using TEE. VVI showed systematically lower strain values than sonomicrometry (bias −0·78%). The opposite could have been expected because VVI tracked the inner border of the phantom, whereas the sonomicrometry crystals were placed on the outer border of the phantom. Moreover, STE, also tracking the inner phantom border, showed significantly higher strain values than sonomicrometry (bias +0·63%).

Although global strain by both methods correlated strongly with the reference values, Tables 1 and 2 show that the two methods are not directly comparable. The bias for both methods was high compared with the measured strain level. The measured strain amplitudes in our aortic phantoms were lower than the previously reported *in vivo* strain values for the human aorta in patients with aortic valve disease (Petrini *et al.*, 2010, 2014). However, this was entirely because of lower flow volumes in the phantoms. When extrapolating the flow volumes by obtained regression formulas of phantom measurements, the resulting strain values were comparable to *in vivo* results. Independent of flow volumes, there were considerable biases between the evaluated techniques, VVI

Table 3 Strain values calculated by regression formulas obtained from the four measurements at lower flow volumes (14–35 ml s^{-1}) shown in Table 1.

Strain	Formula	Peak flow 35 ml s^{-1}	Peak flow 49 ml s^{-1}	Peak flow 98 ml s^{-1}
Phantom 1				
Sono %	0·208 + 0·065*SV	2·483	3·393	6·578
VVI %	−0·576 + 0·069*SV	1·839	2·805	6·186
STE %	0·065 + 0·099*SV	3·530	4·916	9·767
Phantom 2				
Strain				
Sono %	0·105 + 0·069*SV	2·520	3·486	6·867
VVI %	−0·718 + 0·066*SV	1·592	2·516	5·750
STE %	0·035 + 0·095*SV	3·360	4·690	9·345

underestimating, and STE overestimating the sonomicrometry values. We have no explanation for this discrepancy, other than that it must be because of differences in the tracking algorithms or transformation of the tracked data into strain values, because the correlations between the methods were excellent.

Conventional methods for assessment of arterial function usually represent global and not regional arterial function, in contrast to several studies showing inhomogeneous deformation pattern around the circumference of different arteries *in vivo* and *ex vivo* (Petrini *et al.*, 2010; Avril *et al.*, 2011; Kim & Baek, 2011; Yang *et al.*, 2011). Taking this into account, strain imaging could offer a more detailed understanding of arterial function. In general, the regional strain estimation was less accurate than the global strain estimation, which is shown by lower correlation coefficients (Table 2). The regional strain results also varied considerably for the different segments. Sonomicrometry measured the lowest strain in the segment (S_1) closest to the transducer, whereas the highest strain was measured in the segment (S_4) furthest from the transducer. VVI showed a pattern of regional strain similar to that of sonomicrometry, but there was a high variability between the different registrations. The regional strain measured by STE displayed smooth curves, implying good tracking, even when there was a large bias compared with sonomicrometry. No obvious pattern of less accurate tracking in particular segments

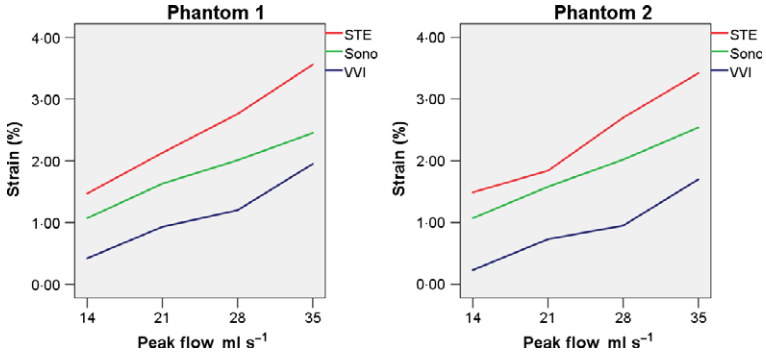

Figure 7 Relationship between peak flow volumes and strain values in the two phantoms. Strain estimated by Sonomicrometry (Sono), VVI and STE.

was found except for S_1 and S_4 by STE, for which no significant correlation between the estimation and reference strain was found. One explanation for the poor performance in S_1 and S_4 may be the fact that the lateral resolution in ultrasound is intrinsically lower than the axial resolution.

There are technique-based variations for estimating strain when using different tracking algorithms. STE is based on tracking a large number of speckles (acoustic markers) (Leitman *et al.*, 2004) and fitting data to a spatial polynomial curve according to the correlations between the original markers and tracked markers using the sum-of-absolute-difference method (Bansal *et al.*, 2008). The basis of VVI is the assumption of the consistency of the tracked geometry by means of Fourier techniques (Pirat *et al.*, 2008). VVI tracking is performed over five-pixel bands and is based on following the reference points, which guide the detection of adjoining points (Bansal *et al.*, 2008; Pirat *et al.*, 2008). Slightly different centre frequencies and frame rates between the methods may also have affected the results. While details of speckle-tracking algorithms developed in-house may be known to the researcher, the details of commercial strain algorithms are unknown to the scientific community. It is therefore not possible fully to understand differences in the results of this study compared with others and the influence of differences in methods for motion analysis (Golemati *et al.*, 2012). Recent guidelines on cardiac chamber quantification report differences between vendors regarding the lower limit of the normal range for global left ventricular strain (Lang *et al.*, 2015). In contrast to the left ventricle, where longitudinal and radial deformation as well as twisting occurs during systole, measuring circumferential strain in an aortic phantom is rather simple. Therefore, the magnitude of difference between VVI and STE was unexpected.

When using commercial strain estimation algorithms, it is important to understand what they were originally intended for. Assessing strain in the aortic wall is likely to be challenging in way that is different from assessing strain in the left ventricular myocardium because of the smaller dimensions and deformations. The absolute estimated deformation might be so small that it is filtered out to some extent by the software filters. Ideally, the same conditions should apply during validation and experimental or clinical use. The dimensions of the phantoms in this study were close to the lower limit of the normal diameter of the descending human aorta (Carrascosa *et al.*, 2013). However, VVI has been used in left ventricular analysis in rats (Wei *et al.*, 2008), implying that the size of the aortic phantom was of minor importance. In STE, a special program for 'small animals' was used.

The temporal resolution and lateral resolution – that is the frame rate and ultrasound centre frequency – are also factors to take into account when using these tracking algorithms. The frame rate was chosen according to recommendations from the manufacturer (>80 Hz), whereas the available TEE transducers limited the choice of the centre frequency. The lateral resolution decreases with increased image depth and depends on the focus position when using a sector probe as in TEE. This was addressed by placing the focus of the ultrasound beam at the far wall of the phantom.

Limitations

A limitation of this study was the fact that reference strain was obtained only from sonomicrometry crystals mounted on the outside of the phantom. Acquiring reference strain values from crystals both on the inside and the outside of the phantom might have produced better comparisons between VVI and STE strain measurements and made measurement of radial strain possible. Radial strain was not our main focus, as our aim was to make a phantom validation mimicking our measurements of descending aortic strain *in vivo* (Petrini *et al.*, 2010, 2014). The reference and estimated strain values were acquired in slightly different short-axis planes to avoid crystal influence on the ultrasound images. However, this should not have introduced any substantial bias because it is reasonable to assume the same movement of the phantom in adjacent parallel planes.

The phantoms were manufactured to resemble the mechanical properties of the aorta (Fromageau *et al.*, 2007). We refrained from surrounding the phantoms with a material that would mimic the descending aorta's anatomical surroundings and minimize dampening of movement introduced by the pulsatile flow. The measured strain values were lower than those measured *in vivo* in patients with aortic valve disease (Petrini *et al.*, 2010, 2014), limited by the maximum flow of the pump, which had a stroke volume smaller than what would be expected in physiological or pathological conditions. However, strain values calculated at estimated similar stroke volumes, as in our previous studies (Petrini *et al.*, 2010, 2014), were comparable to the *in vivo* results. Because the pump could not generate large stroke volumes, it was compensated for using a phantom with an inner diameter of 14 mm, which is smaller than an average adult human aorta but close to the lower limit of the normal inner diameter of the descending aorta ($22{\cdot}3 \pm 4{\cdot}0$ mm) (Carrascosa *et al.*, 2013). Stiffness and distensibility estimates could not be derived in this study because the pressure changes in the phantom could not be measured.

Conclusion

Strong correlations were observed between the global circumferential strain values obtained with VVI and STE and those obtained by sonomicrometry in phantoms that mimicked the descending aorta. These findings support the notion that VVI and STE applied to ultrasound TEE images can be used for the assessment of aortic strain. However, because there are differences in the measured global and regional strain between the tracking methods, this should be taken into consideration

when comparing results from studies using different software for the aortic evaluation.

Acknowledgments

The study was supported by the Swedish Research Council (diary numbers 2011-3579; K2012-65X-22036-01-3), the Swedish Heart Lung Foundation (project numbers 20120209, 20150423), the Stockholm County Council (grant numbers 20120628, 20130301, 20150517) and a donation by Fredrik Lundberg.

Funding

The study was supported by the Swedish Research Council, the Swedish Heart Lung Foundation and the Stockholm County Council.

Conflict of interest

The authors report no actual or potential conflict of interests in relation to this document.

References

Avril S, Schneider F, Boissier C, *et al.* In vivo velocity vector imaging and time-resolved strain rate measurements in the wall of blood vessels using MRI. *J Biomech* (2011); **44**: 979–983.

Bansal M, Cho GY, Chan J, *et al.* Feasibility and accuracy of different techniques of two-dimensional speckle based strain and validation with harmonic phase magnetic resonance imaging. *J Am Soc Echocardiogr* (2008); **21**: 1318–1325.

Bihari P, Shelke A, Nwe TH, *et al.* Strain measurement of abdominal aortic aneurysm with real-time 3D ultrasound speckle tracking. *Eur J Vasc Endovasc Surg* (2013); **45**: 315–323.

Carrascosa P, Capunay C, Deviggiano A, *et al.* Thoracic aorta cardiac-cycle related dynamic changes assessed with a 256-slice CT scanner. *Cardiovasc Diagn Ther* (2013); **3**: 125–128.

Cavalcante JL, Lima JA, Redheuil A, *et al.* Aortic stiffness: current understanding and future directions. *J Am Coll Cardiol* (2011); **57**: 1511–1522.

Cho IJ, Shim CY, Yang WI, *et al.* Assessment of mechanical properties of common carotid artery in Takayasu's arteritis using velocity vector imaging. *Circ J* (2010); **74**: 1465–1470.

D'Hooge J, Konofagou E, Jamal F, *et al.* Two-dimensional ultrasonic strain rate measurement of the human heart in vivo. *IEEE Trans Ultrason Ferroelectr Freq Control* (2002); **49**: 281–286.

Fromageau J, Gennisson JL, Schmitt C, *et al.* Estimation of polyvinyl alcohol cryogel mechanical properties with four ultrasound elastography methods and comparison with gold standard testings. *IEEE Trans Ultrason Ferroelectr Freq Contro* (2007); **54**: 498–509.

Golemati S, Stoitsis JS, Gastounioti A, *et al.* Comparison of block matching and differential methods for motion analysis of the carotid artery wall from ultrasound images. *IEEE Trans Inf Technol Biomed* (2012); **16**: 852–858.

Kim J, Baek S. Circumferential variations of mechanical behavior of the porcine thoracic aorta during the inflation test. *J Biomech* (2011); **44**: 1941–1947.

Kim DH, Kim HK, Kim MK, *et al.* Velocity vector imaging in the measurement of left ventricular twist mechanics: head-to-head one way comparison between speckle tracking echocardiography and velocity vector imaging. *J Am Soc Echocardiogr* (2009a); **22**: 1344–1352.

Kim KH, Park JC, Yoon HJ, *et al.* Usefulness of aortic strain analysis by velocity vector imaging as a new echocardiographic measure of arterial stiffness. *J Am Soc Echocardiogr* (2009b); **22**: 1382–1388.

Lang RM, Badano LP, Mor-Avi V, *et al.* Recommendations for cardiac chamber quantification by echocardiography in adults: an update from the American Society of Echocardiography and the European Association of Cardiovascular Imaging. *Eur Heart J Cardiovasc Imaging* (2015); **16**: 233–270.

Larsson M, Kremer F, Heyde B, *et al.* Ultrasound-based Speckle Tracking for 3D Strain estimation of the Arterial wall — An experimental validation study in a tissue mimicking phantom. In: Ultrasonics Symposium (IUS), 2011 IEEE International (2011), pp. 725–728.

Larsson M, Heyde B, Kremer F, *et al.* Ultrasound speckle tracking for radial, longitudinal and circumferential strain estimation of the carotid artery–an in vitro validation via sonomicrometry using clinical and high-frequency ultrasound. *Ultrasonics* (2015); **56**: 399–408.

Laurent S, Cockcroft J, Van Bortel L, *et al.* Expert consensus document on arterial stiffness: methodological issues and clinical applications. *Eur Heart J* (2006); **27**: 2588–2605.

Leitman M, Lysyansky P, Sidenko S, *et al.* Two-dimensional strain-a novel software for real-time quantitative echocardiographic assessment of myocardial function. *J Am Soc Echocardiogr* (2004); **17**: 1021–1029.

Ma XJ, Duan YY, Yuan LJ, *et al.* Quantitative assessment of maternal common carotid artery mechanics using velocity vector imaging in pre-eclampsia. *Eur J Obstet Gynecol Reprod Biol* (2012); **160**: 30–34.

Mancia G, De Backer G, Dominiczak A, *et al.* Guidelines for the management of arterial hypertension: The Task Force for the Management of Arterial Hypertension of the European Society of Hypertension (ESH) and of the European Society of Cardiology (ESC). *Eur Heart J* (2007); **28**: 1462–1536.

Oishi Y, Mizuguchi Y, Miyoshi H, *et al.* A novel approach to assess aortic stiffness related to changes in aging using a two-dimensional strain imaging. *Echocardiography* (2008); **25**: 941–945.

Perk G, Tunick PA, Kronzon I. Non-Doppler two-dimensional strain imaging by echocardiography–from technical considerations to clinical applications. *J Am Soc Echocardiogr* (2007); **20**: 234–243.

Petrini J, Yousry M, Rickenlund A, *et al.* The feasibility of velocity vector imaging by transesophageal echocardiography for assessment of elastic properties of the descending aorta in aortic valve disease. *J Am Soc Echocardiogr* (2010); **23**: 985–992.

Petrini J, Jenner J, Rickenlund A, *et al.* Elastic properties of the descending aorta in patients with a bicuspid or tricuspid aortic valve and aortic valvular disease. *J Am Soc Echocardiogr* (2014); **27**: 393–404.

Pirat B, Khoury DS, Hartley CJ, *et al.* A novel feature-tracking echocardiographic method for the quantitation of regional myocardial function: validation in an animal model of ischemia-reperfusion. *J Am Coll Cardiol* (2008); **51**: 651–659.

van Prehn J, Vincken KL, Sprinkhuizen SM, *et al.* Aortic pulsatile distention in young

healthy volunteers is asymmetric: analysis with ECG-gated MRI. *Eur J Vasc Endovasc Surg* (2009); **37**: 168–174.

Ribbers H, Lopata RG, Holewijn S, *et al*. Non-invasive two-dimensional strain imaging of arteries: validation in phantoms and preliminary experience in carotid arteries in vivo. *Ultrasound Med Biol* (2007); **33**: 530–540.

Teixeira R, Vieira MJ, Goncalves A, *et al*. Ultrasonographic vascular mechanics to assess arterial stiffness: a review. *Eur Heart J Cardiovasc Imaging* (2016); **17**: 233–246.

Wang L, Wang J, Xie M, *et al*. Clinical study of the ascending aorta wall motion by velocity vector imaging in patients with primary hypertension. *J Huazhong Univ Sci Technolog Med Sci* (2009); **29**: 127–130.

Wei Z, Su H, Zhang H, *et al*. Assessment of left ventricular wall motion in diabetic rats using velocity vector imaging combined with stress echocardiography. *Echocardiography* (2008); **25**: 609–616.

Yang WI, Ha JW. Non-invasive assessment of vascular alteration using ultrasound. *Clin Hypertens* (2015); **21**: 25.

Yang WI, Shim CY, Bang WD, *et al*. Asynchronous arterial systolic expansion as a marker of vascular aging: assessment of the carotid artery with velocity vector imaging. *J Hypertens* (2011); **29**: 2404–2412.